A simulation study of human sensory dynamics and driver-vehicle response

C. J. Nash
Former Research Student

D. J. Cole*

Department of Engineering
University of Cambridge
Cambridge CB2 1PZ, UK
Email: djc13@cam.ac.uk

In previous work a driver model with visual and vestibular sensory dynamics was developed, identified and validated, using data from moving-base driving simulator experiments. In the present paper the predictions, applications and limitations of the driver model are explored through a series of simulations. The aim is to address as yet unanswered questions about the role of visual and vestibular sensory dynamics in the driver-vehicle system. The visual system is found to be the dominant sensory system, with the influence of vestibular measurements increasing with the proportion of random disturbances on the vehicle. State perception errors increase significantly with the proportion of random disturbances on the vehicle. The driver's simulated control performance is unchanged with signal amplitude above perception threshold levels, although it is slightly affected by high-pass filtering of the physical motion such as might be experienced in a driving simulator. The sensory driver model led to a significantly different optimum value of vehicle centre of mass position compared to that obtained using an idealised driver model. The results motivate the adoption of sensory driver models in a vehicle design setting. Further work could be undertaken to improve the sensorimotor noise model.

1 Introduction

Modelling driver steering control mathematically has been a subject of research for several decades. Comprehensive reviews of early methods are provided in [1, 2]. Recent research has focussed on the application of optimal control theory, such as model predictive or linear quadratic controllers that are able to preview the target path and calculate an optimal sequence of control actions to follow the target [3–5]. This control-theoretic approach has been extended to include neuromuscular dynamics [6], and to the control of nonlinear vehicle dynamics [7, 8]. Despite these developments, most models assume the driver has full access to the vehicle states. Few existing driver models take account of human sensory dynamics, sensorimotor noise, and state estimation. For a full review of related work up to 2015 on sensory dynamics and driver modelling see [9].

A human driver can be considered to control a plant consisting of the open-loop vehicle dynamics and the driver's neuromuscular and sensory systems. A parametric model of driver steering control which incorporates human sensory dynamics (visual and vestibular), sensorimotor noise, and state estimation was reported in [10]. A series of experiments was carried out in a moving-base driving simulator in [11,12] to identify and validate the model against measured steering behaviour. The sensory driver model was shown to fit the results of the experiments well, confirming that it is representative of the steering control strategy used by human drivers. The model is a significant extension of previous models that represented an idealised driver. An idealised driver model assumes that the driver has full state feedback, whereas in reality the driver must estimate the plant states based on noisy, filtered and delayed sensory measurements.

More recently, work related to human sensory dynamics in the driver-vehicle system has included use of vestibular dynamics models to optimise motion cueing algorithms for moving-base driving simulators. For example, in [13] a model of the driver's vestibular system was used to quantify perceived acceleration tracking error. In [14] a model predictive control based motion cueing algorithm was used to reduce visual-vestibular discrepancies by up to 33% while maintaining the level of motion scaling and workspace use.

Non-parametric frequency response models identified from driving simulator experiments have been used to obtain insight to a driver's use of sensory feedback. In [15] it was concluded that physical motion in the driving simulator is needed to obtain realistic driving behaviour when the vehicle is subjected to external disturbances. Physical motion

*Address all correspondence to this author.

was found not to be necessary when the driving task involved following a winding road in the absence of external disturbances. Multi-loop frequency response function estimates obtained in [16] revealed how drivers use visual preview of the target path, lateral position feedback, and heading feedback. However in this study there was no physical motion in the driving simulator experiments.

Markkula *et al* [17] presented a simulation framework for intermittent sensorimotor control that is based on a set of neurobiological mechanisms, specifically: (i) ballistic motor primitives, (ii) prediction of sensory responses, and (iii) accumulation of prediction errors. The plausibility of this model was assessed by comparison to data measured from lane-keeping and limit-handling tasks. In [18] the driver model was extended to include mechanisms for sensory integration and behavioural adaptation. However the vestibular model was limited to yaw rate only and did not account for the dynamics of the semicircular canals. Preview of the target path was limited to a single point. The model was used to simulate human steering behaviour in a slalom driving task performed in a moving-base driving simulator with linearly down-scaled motion cues. The model was found to explain effects observed in the driving simulator experiments: decreased task performance and increased steering effort during the early stages of the task, followed by reversal of these effects as the task continued. The neurobiological approach of Markkula *et al* contrasts with the control-theoretic approach usually taken in the field of driver modelling. For example, the parametric driver model in [10] employs an 'internal model' of the vehicle that is used for optimal state estimation and optimal control. In [17, 18] there is no such internal model.

From the review of the literature it appears that the model presented in [10] represents the state-of-the-art in parametric control-theoretic sensory driver models. This model is also cited in [18] as a benchmark for comparison. The aim of the present paper is to use the model to address as yet unanswered questions about the role of visual and vestibular sensory dynamics in the driver-vehicle system. The benefit of using of a parametric model is that potentially greater insight can be obtained compared to a nonparametric frequency response model.

The simulation procedure is described in Section 2 and the simulation conditions are defined in Section 3. Section 4.1 addresses the presently limited understanding of the role of visual and vestibular sensory feedback in a combined path-following and disturbance-rejection steering task. A novel parameter, the forcing function gain, is introduced to quantify the proportion of the task that is path-following. The results complement and explain the experimental findings in [15]. In addition, the effect of motion scaling (typically present in a driving simulator) on the relative contributions of visual and vestibular sensory feedback is quantified, and the effect of the forcing function gain on the accuracies of the driver's perception of motion state and slip angle are calculated; these findings from the model provide new insight to the role of sensory feedback and state estimation in driver perception.

In Section 4.2 the RMS path-following error and the RMS handwheel steering angle predicted by the model are used to further quantify the effect of visual and vestibular sensory feedback on path-following and disturbance-rejection tasks. In addition, the model is used to provide new insight to the finding in [12,19] that drivers in a moving-base simulator may not always correctly account for high-pass filtered motion, and instead drive as though the motion were scaled.

Despite the previously published work in modelling driver sensory dynamics there is little indication of the extent to which vehicle parameter optimisation in the driver-vehicle system might be affected. While it is not possible within the scope of the paper to explore the full design space of a vehicle, one parameter (the longitudinal position of the centre of mass) is examined in Section 4.3. The results motivate the inclusion of sensory dynamics in driver-vehicle optimisation studies.

Some limitations of the sensory driver model are discussed in Section 5. Conclusions and suggestions for further work are given in Section 6.

This paper is derived from Chapter 7 of [20] and most of the figures are from that document. Preliminary results were reported in [21].

2 Driver-vehicle model

The driver-vehicle model is shown in Fig. 1. The plant consists of the vehicle dynamics and the driver's neuromuscular dynamics and sensory dynamics. The driver control is represented by a linear quadratic regulator (LQR) with a Kalman filter operating on an 'internal model' of the plant. The plant is shown in more detail in Fig. 2. Full details and parameter values are given in [10–12, 19] and in the data repository (link given in the acknowledgement), but a brief description is provided in the remainder of this section to enable the reader to interpret the results given in the paper.

Beginning at the left-hand side of Fig. 2, the LQR controller output with added neuromuscular process noise passes through the driver's neuromuscular dynamics $H_{nms}(s)$, represented by a second order low-pass filter, giving the handwheel steering angle input δ to the vehicle. The natural frequency (10rads^{-1}) and damping ratio (0.54) of the filter were identified from driving simulator experiments [11]. Steering torque feedback from tyre lateral forces is not included in the model (and was not present in the driving simulator used for identification).

The vehicle dynamics $H_V(s)$ are represented by a constant speed, linear single-track 'bicycle' model with two degrees-of-freedom. The input is the handwheel steering angle δ and the outputs are the lateral (sideslip) velocity $\hat{v}$ at the centre of mass and the yaw velocity $\hat{\omega}$. The vehicle model is parameterised by: mass (650kg); yaw moment of inertia (450kgm^2); front and rear axle distances to the centre of mass (1.85m, 1.65m); front and rear cornering stiffnesses ($100\text{kNrad}^{-1}, 230\text{kNrad}^{-1}$); and steering gear ratio (10). The given baseline parameter values represent a high-performance single-seat racing car, and were identified

from driving simulator experiments [11]. For the nonlinear simulations in Subsection 4.1.3 the linear tyres are replaced by nonlinear tyres. Lateral and yaw velocity motion disturbances f_v and f_ω are generated by low-pass filtering uncorrelated white noise sources w_v and w_ω. The resulting lateral velocity v and vehicle yaw angular velocity ω are transformed to vehicle yaw angle ψ, lateral displacement y and lateral acceleration a, according to the forward speed of the vehicle U. In the case of a moving-base driving simulator instead of a real vehicle, the vehicle's true lateral acceleration and yaw angular velocity may be scaled and/or high-pass filtered using $H_{ma}(s)$ and $H_{m\omega}(s)$.

The vestibular organs are the otoliths and semi-circular canals (SCCs), with dynamics $H_{oto}(s)$ and $H_{SCC}(s)$. They sense vehicle lateral acceleration and yaw angular velocity, with a vestibular delay of τ_{ve}, giving sensed lateral acceleration a_{ve} and yaw angular velocity ω_{ve}.

A target path lateral displacement f_t is generated by filtering white noise source w_t. The driver looks ahead as far as the prediction horizon and previews the target path f_t relative to the vehicle's longitudinal axis. The visual measurements are: (i) the lateral distance of the vehicle from the target path e; and (ii) the angle of the target path relative to the vehicle's longitudinal axis measured at equally spaced points up to the prediction horizon, denoted by the array $\boldsymbol{\varphi}$. The visual measurements are delayed by τ_{vi} to give sensed lateral displacement e_{vi} and sensed angles $\boldsymbol{\varphi}_{vi}$.

Returning to Fig. 1, white sensory measurement noise is added to the outputs of the plant, and white neuromuscular process noise is added to the output of the controller. The model identification and validation exercise [11] indicated that the white noise assumption was not valid at frequencies much above the bandwidth of the driver's control action (> 3Hz). However, in the frequency range of the driver's control action the white noise assumption was judged to be reasonable.

A Kalman filter represents the driver's state estimation function. A linear quadratic regulator (LQR) represents the driver's optimal control action. The LQR acts to minimise a weighted sum of the squared path-following lateral displacement error e and the square of the controller output $\hat{\delta}$. Various driver control strategies are obtained by fixing the weight on path error q_e to unity and adjusting the weight on controller output $q_{\hat{\delta}}$. Other signals could be added to the cost function, such as steering rate and path-following heading error, but the model identification and validation exercise indicated that the chosen signals were appropriate. Adding more signals to the cost function would increase the risk of overfitting.

The driver-vehicle model was extensively identified and validated using measured data collected from driving simulator experiments [10–12, 19]. The driving simulator was equipped with a high-bandwidth motion base. Test subjects with a range of driving experience were asked to steer the vehicle along a target path under a range of conditions. The conditions encompassed: vehicle speed; stochastic or transient vehicle motion disturbances; linear or nonlinear tyres; scaled and/or high-pass filtered physical motion cueing; straight line, random, lane change or large angle target paths. The model parameters identified from the measured data included: LQR cost function weight; sensory noise variances; process noise variance; preview time; vestibular time delay; visual time delay; neuromuscular natural frequency and damping ratio. Model predictions of steering angle matched experimental results well, with a variance accounted for typically 90% of the linear component of measured response. The identified parameter values were physically plausible compared with values from the literature. Subjective assessments of the subjects were recorded for the experiments involving motion filtering [12]; it was found that the higher the drivers rated the usefulness of the physical motion cueing, the more they used their vestibular measurements to control the vehicle. The subjective ratings also correlated with path-following error, with drivers able to follow the target path more closely for physical motion cues that were subjectively assessed as more useful.

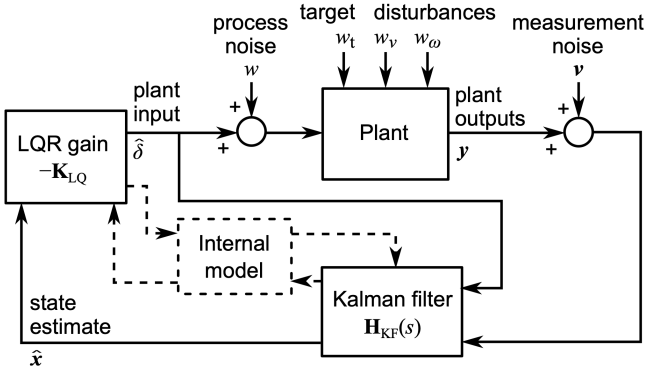

Fig. 1. Driver-vehicle model [10].

The simulations in this paper are generally performed in the frequency domain. Experimental results from [11] indicate that the process noise magnitude W depends linearly on the magnitude of the steering angle RMS(δ), with a constant signal-to-noise ratio SNR_W. Similarly, in [12] measurement noise is found to be signal-dependent, with constant SNRs for each sensory channel plus thresholds η below which the noise magnitude remains constant. When fitting the driver model to experimental results in this previous work, the RMS signal magnitudes were taken directly from the measurements. However, when running simulations without corresponding measurements these RMS values are not known until after the simulation. An iterative procedure is used to achieve a set of RMS signal and noise magnitudes with desired SNR. The procedure converges except when the driver-vehicle system is unstable.

3 Baseline simulation conditions

A baseline set of conditions is defined, which is used for all simulations in Section 4 except where otherwise stated. Many of the conditions are chosen to match those used in the earlier work. The vehicle parameters are those given for the baseline vehicle in Section 2 and [10, 11], with a constant longitudinal speed $U = 40$ m/s. Disturbances are added di-

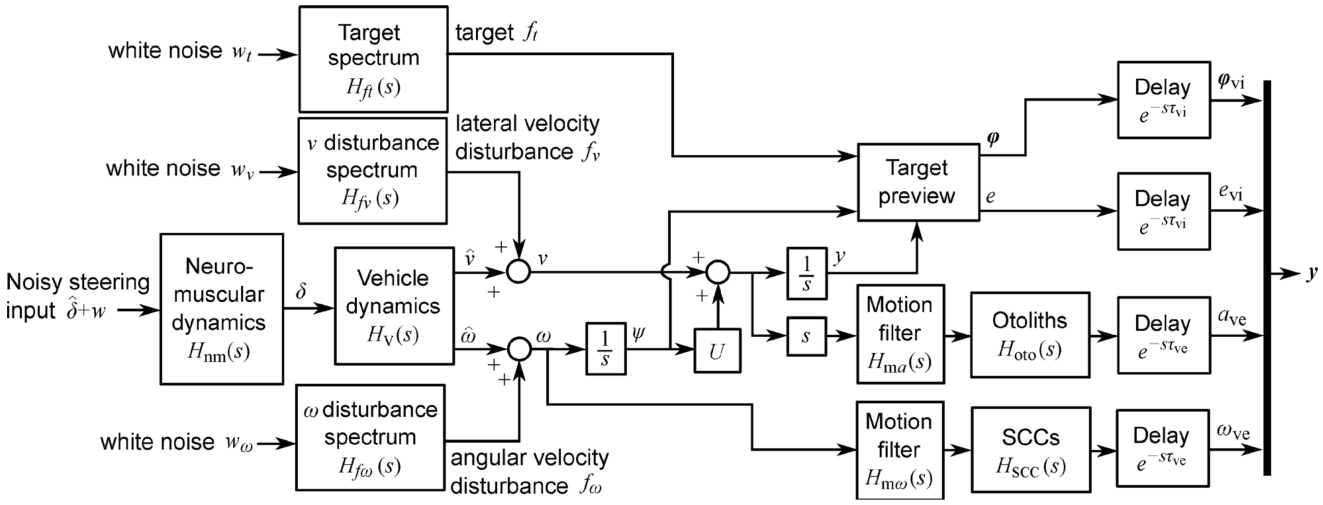

Fig. 2. Plant model [10, 12].

rectly to the lateral and yaw velocities as described in [19]. In simulations of the nonlinear driver model, the parameters for an understeering vehicle with 'nonlinear increasing tyre' are from [10].

In [19] it was found difficult to define a fixed set of signal-to-noise ratios to model a driver's response to transient disturbances, since the noise magnitudes are dependent on the characteristics of the transient signals. Therefore except where stated all simulations in Section 4 are performed in the frequency domain and use filtered white noise target and disturbance signals instead of deterministic transient signals. This is a useful approach for vehicle design and evaluation, since the results depend only on the general statistical properties of the target and disturbance signals rather than on one specific realisation.

The disturbance filters $H_{fv}(s)$ and $H_{f\omega}(s)$ are defined in [19], with RMS input magnitudes $W_v = 30$ m/s^2* and $W_\omega = 25$ rad/s^2* (here, and subsequently, * indicates that the units relate to the output rather than the input to the filters). These values match the spectra of the disturbances used in [19], and each disturbance requires a similar level of steering response from the driver. The target filter is chosen to give a curvature profile similar to a typical road:

$$H_{f\kappa}(s) = \left(\frac{1}{s+1}\right)^2 \tag{1}$$

with $W_\kappa = 0.15$ m^{-1}*. To represent driving a real car (rather than a driving simulator), motion filters $H_{ma}(s)$ and $H_{m\omega}(s)$ are set to unity.

Most of the driver parameters are set to the identified values given in [12]. Following the results in [19], the signal to noise ratio of the target path angle relative to the vehicle SNR_ϕ is set equal to 1.04, with the signal magnitude M_ϕ defined as $\mathrm{RMS}(\phi_0)$, where ϕ_0 is the target path angle relative to the vehicle. All other signal magnitudes are defined by the RMS values found using the iterative procedure mentioned in Section 2. A value of 1 is used for the LQR controller's cost function weighting q_δ on the mean square of the steering angle δ, which is a reasonable average of values found in the earlier work. In general it is assumed that the driver has a perfect internal model of the plant, although a few simulations explore the implications of internal model discrepancies by replacing the motion filters with equivalent scaling factors (ESF) as described in Section 4.2.3. Simulations are also run for an idealised driver model, which has full state feedback and no process or measurement noise. This removes the effects of sensory dynamics and delays.

4 Simulations and results

The simulations are designed to address as yet unanswered questions about the role of visual and vestibular sensory dynamics in the driver-vehicle system. The questions are split into three categories: those relating to the driver's perception are presented in Section 4.1; results concerning the performance of the driver are shown in Section 4.2; the implications of using the new model for the design of vehicles are investigated in Section 4.3.

4.1 Perception

4.1.1 Effect of the sensory measurements on the driver's control

A Kalman filter is used in the model to represent the driver's integration of sensory measurements from their visual and vestibular systems. The measurements are combined to give an optimal state estimate based on an internal model of the plant and estimates of the process and measurement noise magnitudes. Using the proportional relationship between signal and noise magnitudes identified in previous work, it is possible to use the driver model to explore how each sensory measurement is used under different operating conditions.

Transfer functions can be found between each of the sensory measurements and the simulated steering angle, us-

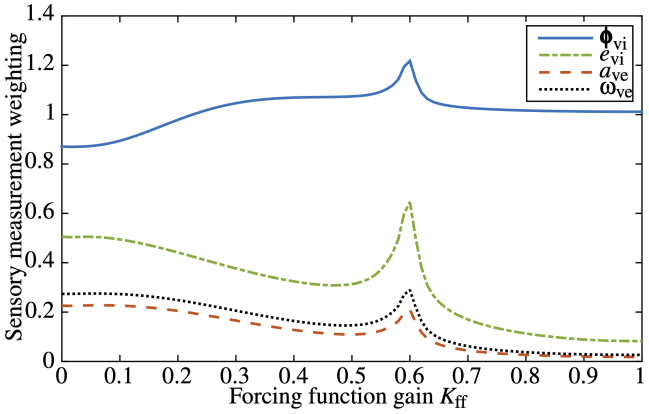

Fig. 3. Sensory weightings for various target and disturbance forcing function amplitudes. Weightings show the proportion of steering angle RMS resulting from each sensory measurement with the task varying between disturbance-rejection ($K_{ff} = 0$) and target-following ($K_{ff} = 1$). The sensory measurements are (top to bottom) visual target angles, visual lateral path error, vestibular lateral acceleration, vestibular yaw velocity.

ing the principle of linear superposition to decompose the steering signal into contributions from each sensory measurement. The procedure described in Section 3 is used to calculate the expected RMS values of the steering angle contribution from each sensory measurement. These values are then divided by the total expected steering angle RMS in order to give a measure of the relative contribution, or weighting, of each of the sensory measurements.

To investigate how a driver's use of sensory measurements depends on the control task, relative weightings are found for various target and disturbance forcing function amplitudes. A forcing function gain K_{ff} is varied from 0 to 1, such that $W_\kappa = 0.15K_{ff}$ m^{-1}*, $W_v = 30(1-K_{ff})$ m/s^2* and $W_\omega = 25(1-K_{ff})$ rad/s^2*. This gives a task which transitions from disturbance-rejection only at $K_{ff} = 0$ (driver steers the vehicle to follow a straight target path while compensating motion disturbances of the vehicle) to target-following only at $K_{ff} = 1$ (driver steers the vehicle to follow a randomly curving target path but there are no motion disturbances of the vehicle).

The relative weightings of the sensory measurements for various target and disturbance forcing function amplitudes are shown in Fig. 3. The weightings can add up to more than 1 because the contributions of the measurements can be out of phase with each other and so combine destructively. For all values of the forcing function gain the visual measurements, particularly the previewed target angles $\boldsymbol{\varphi}_{vi}$, are weighted more highly than the vestibular measurements. This is consistent with the intuitive idea that it is much easier to drive with no physical motion feedback than with no visual measurements.

For the target-only task ($K_{ff} = 1$) the weighting of the previewed target angles is close to 1 while the vestibular measurements and the visually-perceived lateral path error contribute very little to the driver's steering action. This is because the driver can look ahead at (preview) the upcoming target path and calculate an optimal control action. The absence of vehicle motion disturbances, and the presence of an internal model that exactly matches the plant, mean that there is little benefit in measuring the vehicle motion states. However there is a small non-zero weighting on the vestibular measurements, which contributes to the feedback control necessary to compensate the driver's process and measurement noise. There is also a small weighting on visually-perceived lateral path error, which is necessary to prevent drift of the vehicle away from the target path. The small weighting on vestibular measurements for a target-only task is consistent with the experimental findings in [15].

As the task becomes increasingly disturbance rejection the influence of the vestibular measurements tends to increase while the previewed target angle weighting tends to decrease. There is a peak in all weightings for K_{ff} around 0.6, where the various sensory measurements interact particularly destructively. For the disturbance-only task ($K_{ff} = 0$) the vestibular measurements are each weighted about a quarter as much as the previewed target angles. In contrast to the target angles the motion disturbances cannot be previewed. The driver must therefore rely on feedback control to compensate the motion disturbances, and the vestibular measurements of the vehicle motion states provide significantly useful information. Although the target path in this case ($K_{ff} = 0$) is a straight path, it is still important for the driver to preview and follow the target path, and so the weighting on the target angles is still the largest of the measurements. The non-negligible weighting on vestibular measurements for a disturbance rejection task is consistent with the experimental findings in [15].

To investigate how a driver's use of sensory measurements is affected by motion signal amplitude, relative sensory weightings are also found with the lateral and yaw physical motion scaled by various factors from 0 to 1, as might be required in a moving-base driving simulator. The results are shown in Fig. 4 for a forcing function gain $K_{ff} = 0.5$. For motion signals which are above perception threshold levels, the sensory weightings are independent of signal amplitude. This is a result of the signal-dependent measurement noise; when the signal amplitude increases the noise level increases in proportion, therefore the uncertainty of the signal is unchanged. Below perception threshold levels the sensory weightings decrease approximately linearly to zero, and the weightings of other sensory measurements vary slightly to compensate.

4.1.2 Accuracy of the vehicle states estimated by the driver

The driver model can be used to investigate how accurately a driver is able to estimate the states of the vehicle, depending on the simulated driving task and the driver noise amplitudes. This can be quantified by finding the perception error, defined as the difference between the true and estimated states. The procedure outlined in Section 3 is used to calculate the expected RMS perception error for the two

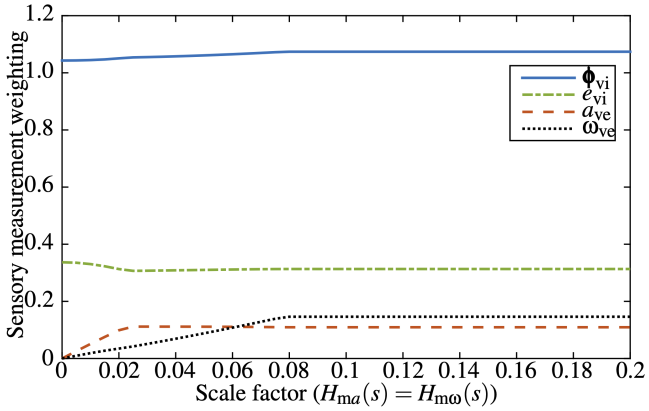

Fig. 4. Sensory weightings with various scaling factors on the physical motion. Forcing function gain $K_{ff} = 0.5$. The sensory measurements are (top to bottom) visual target angle, visual lateral path error, vestibular lateral acceleration, vestibular yaw velocity.

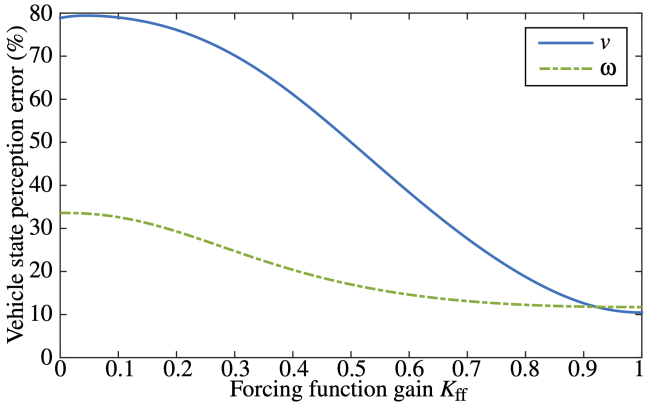

Fig. 5. Vehicle state perception error with various forcing function amplitudes, defining a task which varies between disturbance-rejection ($K_{ff} = 0$) and target-following ($K_{ff} = 1$).

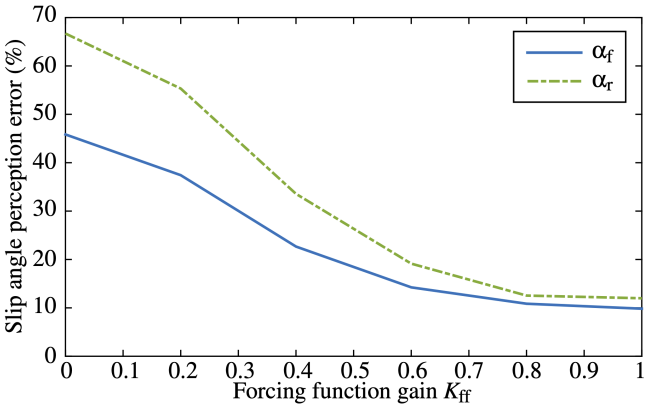

Fig. 6. Slip angle perception error with various forcing function amplitudes, defining a task which varies between disturbance-rejection ($K_{ff} = 0$) and target-following ($K_{ff} = 1$).

vehicle states, v and ω. Target and disturbance amplitudes are varied by changing K_{ff} in a similar way to the results presented in Fig. 3. The expected perception errors are plotted as a percentage of the total expected RMS value of each state in Fig. 5. The perception errors are largest for the disturbance-rejection only task ($K_{ff} = 0$), because the motion disturbances on the vehicle make prediction of the vehicles states inaccurate. The perception error in ω is much smaller than in v, this will depend on the conditions of the simulation such as the vehicle dynamics and the properties of the disturbances. The perception errors decrease as the disturbance-rejection component decreases ($K_{ff} > 0$). When $K_{ff} = 1$ there are no vehicle motion disturbances and the error in the state estimates are determined by the process and measurement noise, and are around 10% of the total signal. Although the target path disturbance increases with K_{ff}, the target path disturbance itself does not affect the accuracy of the vehicle motion state estimates. Simulations are also carried out with varying motion scaling factors, and the perception errors are found to remain constant for motion above the perception threshold levels, similarly to the results seen in Fig. 4.

4.1.3 Effect of the sensory dynamics on a driver's estimate of the operating point of a nonlinear vehicle

When controlling a nonlinear vehicle it is even more important for the driver to be able to estimate the vehicle states correctly. This is because the nonlinear vehicle responds differently to steering inputs as the operating point changes. For the constant-speed vehicle with nonlinear tyres tested in [19], the operating point of the vehicle can be defined by the front and rear slip angles α_r and α_f. Results from an experiment carried out in a simulator in [19] showed that real drivers can account for the time-varying operating point of a nonlinear vehicle.

Simulations of the nonlinear driver model are run to determine how sensory dynamics affect a driver's ability to estimate the front and rear slip angles of a nonlinear vehicle. Similarly to the results presented in Fig. 5, the forcing function gain K_{ff} is varied from 0 to 1 to change the task from disturbance-rejection to target-following. The RMS perception error for the front and rear slip angles is found in each case as a percentage of the total RMS value of each slip angle. The procedure outlined in Section 3 to calculate expected values cannot be used for a nonlinear model, therefore simulated white noise signals are used as inputs to a time domain simulation of the driver and vehicle model.

The resulting slip angle perception errors are shown in Fig. 6. Similarly to the state perception errors shown in Fig. 5, the slip angle perception errors increase with vehicle motion disturbance amplitude. For pure target-following ($K_{ff} = 1$) the slip angles are estimated with an error of around 10%, arising from the driver's process and measurement noise. With the conditions tested the front slip angle is estimated more accurately than the rear slip angle, this will depend on the vehicle dynamics and the properties of the disturbances.

4.2 Performance

It is important to understand how the closed-loop driver-vehicle system will perform under different conditions, in order to predict how drivers will react and to design vehicles to achieve a desired performance level. It is expected that inclusion of sensory dynamics in a driver model will result in a more realistic representation of the performance of a real driver.

4.2.1 Bandwidth of a driver's reaction to target and disturbance signals

It has been observed that drivers are limited in the bandwidth of control actions they can apply to a vehicle. The bandwidth is determined by the dynamics and delays of the neuromuscular system, sensory system and the cognitive process [22, 23].

The linear driver model is used to investigate how well drivers are able to respond to different frequencies contained within white noise target and vehicle motion disturbance signals. The forcing function filters are all set to unity, with $W_\kappa = 0.01$ m^{-1}*, $W_v = 10$ m/s^2* and $W_\omega = 10$ rad/s^2*. For each forcing function signal the PSD of the path-following error $S_e(\omega)$ is found both with and without driver steering control. The ratio between these PSDs is then calculated to demonstrate the proportion of the forcing function signals which cannot be controlled by the driver. The simulation is run for three steering angle weightings in the LQR cost function of $q_\delta = 0.1$, 1 and 10.

The results are shown in Fig. 7. For the target forcing function f_κ the driver is able to follow all low-frequency components, however they are unable to follow components above 15 rad/s at all. The proportion of target components followed at frequencies between 0 and 15 rad/s depends on the steering cost weight, with a lower weight resulting in better target-following, as expected.

For the disturbance forcing functions f_v and f_ω the results are more surprising. The driver is similarly able to remove the effects of the lowest-frequency disturbances, and is unable to respond to high-frequency disturbances. However, some of the effects of disturbances in the mid-frequency range are amplified by the driver, which seems like a poor control strategy. However, the results disguise the fact that the most of the path error has low frequency content, thus a control strategy that minimises RMS path error can result in increases in the path error PSD at higher frequencies.

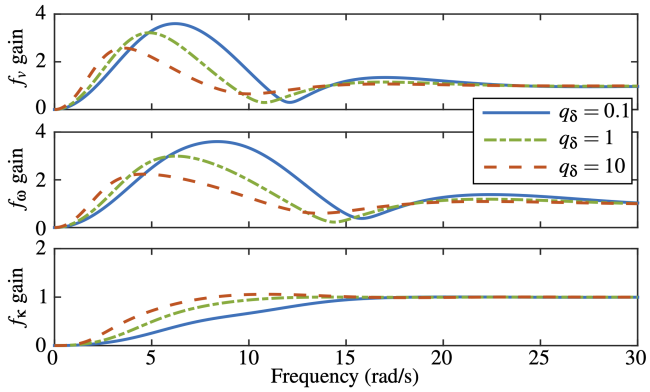

Fig. 7. Bandwidth of driver responses to target and disturbance signals. Results are presented as a gain which is the ratio between the PSDs of path-following error e with and without driver control.

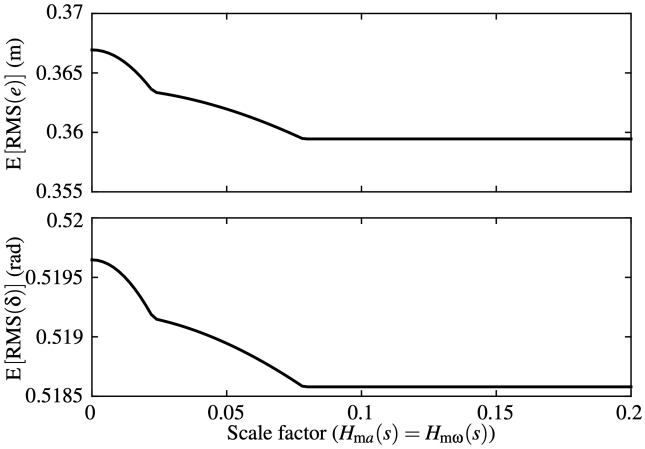

Fig. 8. Expected RMS path-following error e and steering angle δ with different motion scaling factors

4.2.2 Driver performance in a simulator compared to a real vehicle

The increasing availability of high-performance driving simulators has resulted in a large amount of vehicle validation taking place in a simulated environment. This allows new concepts and designs to be tested relatively quickly and cheaply. However, since simulators are limited in their ability to reproduce physical motion, with some having a fixed base, the sensory signals perceived by the driver's vestibular system in a simulator will be different to those perceived in a real car. The driver model can be used to investigate whether this affects the steering performance of the driver, and the extent to which measurements taken in a simulator are applicable to a real vehicle.

The expected RMS path-following error and steering angle are calculated with various scaling factors applied to the physical motion feedback, to represent a simulator with scaled (or no) motion. All other conditions are set to the values defined in Section 3, and it is assumed that the driver has a perfect internal model of the plant, including the scaling factors. The results are shown in Fig. 8. The driver's performance is independent of the scaling factor if the motion is above perception threshold levels, similarly to the driver's weighting of the sensory measurements shown in Fig. 4. For simulators with no or sub-threshold motion, the RMS path-following error and steering angle increase slightly as expected. However the difference is small, showing that drivers are able to achieve a good level of path-following performance with visual feedback only.

To investigate how drivers perform in simulators with filtered motion, further simulations are carried out with high-pass motion filters given by:

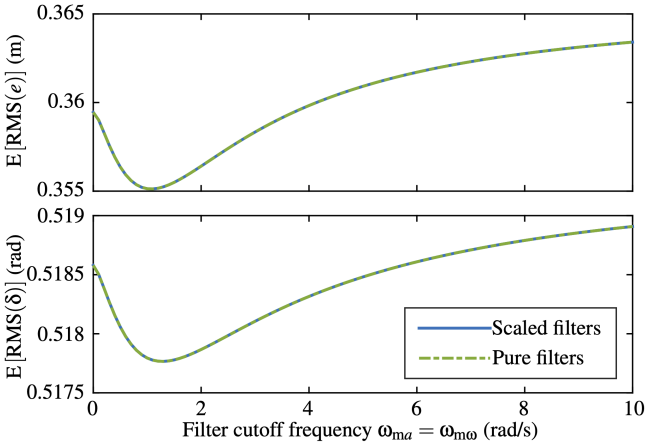

Fig. 9. Expected RMS path-following error e and steering angle δ with different cutoff frequencies. Scaling of the physical motion feedback has no effect on the RMS responses e and δ.

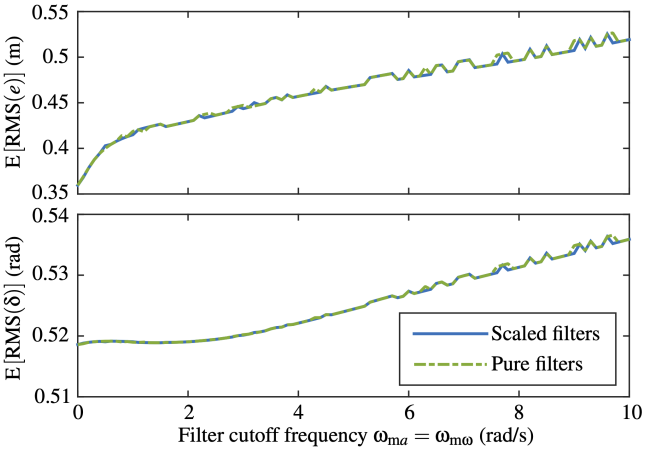

Fig. 10. Expected RMS path-following error e and steering angle δ with different cutoff frequencies, using ESFs in place of motion filters in the driver's internal model

$$H_{\mathrm{m}a}(s) = K_{\mathrm{m}a}\left(\frac{s}{s+\omega_{\mathrm{m}a}}\right)^2 \tag{2}$$

$$H_{\mathrm{m}\omega}(s) = K_{\mathrm{m}\omega}\left(\frac{s}{s+\omega_{\mathrm{m}\omega}}\right)^2 \tag{3}$$

with the cutoff frequency $\omega_{\mathrm{m}a} = \omega_{\mathrm{m}\omega}$ varied between 0 and 10 rad/s. For each cutoff frequency two conditions are tested: 'pure' filters with $K_{\mathrm{m}a} = K_{\mathrm{m}\omega} = 1$ and 'scaled' filters, where $K_{\mathrm{m}a}$ and $K_{\mathrm{m}\omega}$ are chosen to give expected signal amplitudes $\mathrm{E}[\mathrm{RMS}(a_{\mathrm{ve}})] = 0.3$ m/s^2* and $\mathrm{E}[\mathrm{RMS}(\omega_{\mathrm{ve}})] = 0.03$ rad/s* for all cut-off frequencies. These signal amplitudes are specified to be significantly reduced compared to the unfiltered and unscaled motion, but approximately 50% higher than the threshold values. They are achieved with scaling factors < 1. The resulting expected RMS path-following error and steering angle are plotted in Fig. 9, showing that the performance of the driver varies with the frequency content of the physical motion feedback. The best driver performance is not achieved with full motion ($\omega_{\mathrm{m}a} = \omega_{\mathrm{m}\omega} = 0$), since the lowest frequencies contribute significantly to the RMS signal amplitude, increasing the noise amplitude due to the signal-dependent relationship without giving the driver much useful information about the vehicle dynamics. Figure 9 shows that scaling the filtered motion does not affect the performance of the driver. This again is due to the proportional signal-noise relationship, similar to the results shown in Fig. 8. Further discussion into whether this is a realistic result is presented in Section 5.

4.2.3 Effect of an incorrect internal model on driver performance

Results from [12, 19] show that under some circumstances drivers can have difficulty learning an accurate internal model of the plant. In particular, it is found that drivers may not correctly account for filtered motion, and instead drive as though the motion is scaled. Modelling this requires substituting the real motion filters $H_{\mathrm{m}a}(s)$ and $H_{\mathrm{m}\omega}(s)$ with 'equivalent scaling factors' (ESFs) in the driver's internal model of the filters, $H'_{\mathrm{m}a}(s)$ and $H'_{\mathrm{m}\omega}(s)$. To investigate how such a misunderstanding of the motion filtering may affect a driver's control performance, a procedure is defined to find ESFs for a given set of filtering conditions.

The results found in [12, 19] do not give a clear indication of how ESFs depend on the properties of the motion filters. It is plausible that the driver might judge the scaling of the motion based on differences between the RMS values of motion perceived through their visual and vestibular systems. One way to model this is to define the ESFs as the ratio between the expected RMS values of the signals perceived by the vestibular system with motion filters and the expected values with full motion (no motion filters). This can be written mathematically as:

$$H'_{\mathrm{m}a}(s) = \frac{\mathrm{E}[\mathrm{RMS}(a_{\mathrm{ve}})]}{\mathrm{E}[\mathrm{RMS}(a_{\mathrm{ve}}) \mid H_{\mathrm{m}a}(s) = 1]} \tag{4}$$

$$H'_{\mathrm{m}\omega}(s) = \frac{\mathrm{E}[\mathrm{RMS}(\omega_{\mathrm{ve}})]}{\mathrm{E}[\mathrm{RMS}(\omega_{\mathrm{ve}}) \mid H_{\mathrm{m}\omega}(s) = 1]} \tag{5}$$

The effects of varying the motion filter cutoff frequency on the performance of a driver with an incorrect internal model of the motion filters are analysed using simulations similar to the results presented in Fig. 9, replacing the motion filters in the internal model with ESFs. The results of the simulations are shown in Fig. 10. Comparison of Fig. 10 with Fig. 9 shows when the cutoff frequency is zero ($\omega_{\mathrm{m}a} = \omega_{\mathrm{m}\omega} = 0$), the results are the same in both Figures, since the motion filter is unity gain and the ESFs are 1, therefore the internal model is correct. However, as the filter cutoff frequency increases from zero the performance of the driver with the incorrect internal model degrades significantly compared to the driver with correct internal model

Table 1. Expected RMS δ and e for: visual and vestibular feedback; visual feedback only; full state feedback.

	Target only		**Disturbances only**	
	$\mathrm{E}[\mathrm{RMS}(\delta)]$ (rad)	$\mathrm{E}[\mathrm{RMS}(e)]$ (m)	$\mathrm{E}[\mathrm{RMS}(\delta)]$ (rad)	$\mathrm{E}[\mathrm{RMS}(e)]$ (m)
Visual-vestibular	0.47688	0.16324	0.19347	0.28134
Visual only	0.47692	0.16405	0.20228	0.30188
Full state	0.46245	0.02738	0.07008	0.01225

of the motion filters. For example, at a cutoff frequency of 6 rad/s[1] the RMS path error is increased by about 30% due to the incorrect internal model. Scaling the filtered motion does not further affect the performance of the driver, as also seen in Fig. 9. In Fig. 10 the plotted lines are slightly jagged due to small numerical inconsistencies when calculating the ESFs. These simulation results indicate the importance of providing motion filters in moving-base driving simulators that the driver is able to identify.

4.2.4 Influence of the vestibular system on a driver's performance

Simulations in Section 4.1.1 show that vestibular measurements are used primarily for disturbance-rejection during driving. To understand further how vestibular measurements affect the steering control performance of drivers, simulated steering angles and path-following errors are plotted in Fig. 11 for models with and without vestibular dynamics, compared against an idealised driver model with full state feedback. Full state feedback means that the driver has full knowledge of the system states, removing any effects of delays, filters and noise. These signals are created for a trial with a target path only ($W_v = 0$ m/s^2*, $W_\omega = 0$ rad/s^2*) and a trial with vehicle motion disturbances only ($W_\kappa = 0$ m^{-1}*).

Figure 11 shows that there are significant differences between steering angles and path-following errors predicted using models which include sensory dynamics and those predicted by a model with full state feedback. Smaller differences are also seen between models with and without vestibular dynamics. These differences are more significant for disturbance-rejection than for target-following, supporting the finding in Section 4.1.1. Expected RMS values of δ and e for each model are given in Tab. 1. The model with full state feedback steers less and follows the target much more closely than a more realistic model which incorporates sensory dynamics. Using vestibular measurements also allows the driver to steer less with lower path-following error, although once again this effect is more significant when there are disturbances. This shows that drivers use their vestibular system to improve the disturbance-rejection component of their steering performance.

4.3 Vehicle design

Previously published work in modelling driver sensory dynamics gives little indication of the extent to which vehicle parameter optimisation in the driver-vehicle system might be affected by sensory dynamics. This section explores how the driver model can be used to optimise the design of a vehicle, considering the closed-loop driver-vehicle system. The results are compared with predictions from an idealised driver model which does not consider sensory dynamics.

4.3.1 Effect of sensory dynamics on optimal car design

The optimisation of a single vehicle design parameter can be used to illustrate the effect when sensory dynamics are included in a driver model. The objective of the optimisation is to minimise the expected RMS path-following error $\mathrm{E}[\mathrm{RMS}(e)]$. The linear vehicle is used, and for simplicity only one parameter is varied. The variable parameter is the position of the centre of mass of the vehicle, defined by the distance from the centre of mass to the rear axle l_r and choosing the distance to the front axle l_f such that $l_\mathrm{f} + l_\mathrm{r} = 3.5$ m. The default position is $l_\mathrm{r} = 1.65$ m. The remaining vehicle parameters, the target and disturbance signals, and the cost function weight are fixed to the default conditions described in Section 3. Results using the driver model with sensory dynamics are compared with results from an idealised driver model with full state feedback to indicate how the inclusion of sensory dynamics in the driver model affect the optimum centre of mass position. The results presented here are not intended to provide design guidance for centre of mass position; the purpose is to determine the extent to which an exemplar driver-vehicle design optimisation might be affected by the presence of sensory dynamics in the driver model.

The results of the simulations are shown in Fig. 12. Note that the centre of mass position is varied from the rear axle position to the front axle position; this is clearly a much larger range of position than is realistic, but nevertheless it can be useful in the simulation environment to explore what happens at the extremes. It is clear that including sensory dynamics results in a significantly different prediction to the idealised driver model. The expected path-following error is much lower overall for the idealised driver, which is expected as this model is unaffected by driver noise and is able to respond to disturbances instantly. The optimal centre of mass position predicted using the model with sensory dynamics is 0.9 m in front of the optimal position predicted by the idealised driver model. The idealised driver model predicts that the optimal centre of mass position is close to the rear of the vehicle, however the performance of the model with sensory dynamics becomes rapidly worse as l_r decreases below 1 m.

The differences between the predictions of the model with sensory dynamics and the ideal driver model can be explained by considering how moving the centre of mass affects the open-loop response of the vehicle. The vehicle becomes less stable as l_r decreases, and is unstable for $l_\mathrm{r} < 0.24$ m. Fig. 12 shows that the ideal driver is able to stabilise the vehicle effectively, and benefits from the increased vehicle response for a given steering input at low values of

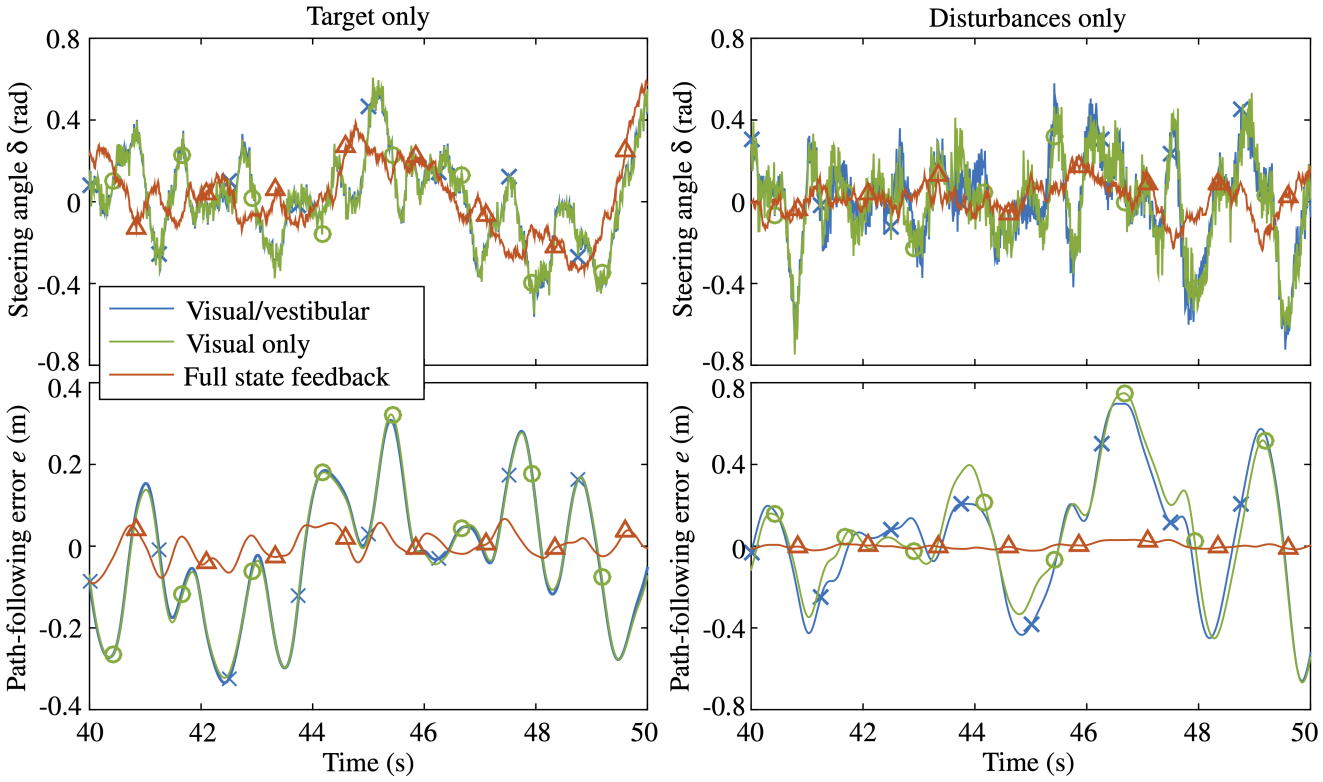

Fig. 11. Effect of vestibular system on steering angle δ and path-following error e. Simulated signals predicted by the driver model are compared for trials with a target only (no disturbances) and disturbances only (straight line target). Blue cross: visual/vestibular; green circle: visual only; red triangle: full state feedback.

l_r. However, the model with sensory dynamics predicts that the driver will have difficulty controlling the vehicle when it gets close to instability, resulting in large path-following error. In practice, real vehicles are usually designed to have a generous margin of open-loop stability.

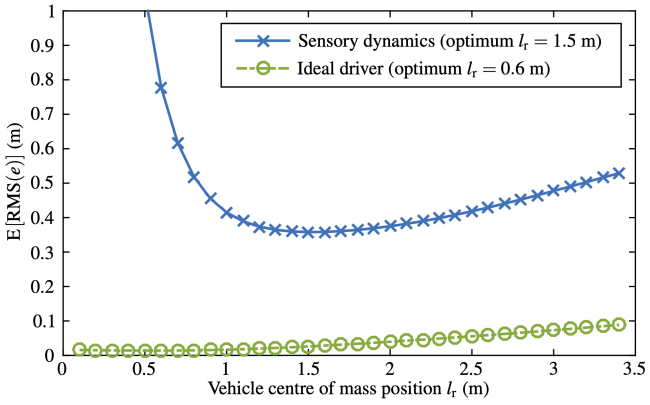

Fig. 12. Optimal centre of mass position with or without sensory dynamics. The expected RMS path-following error e is calculated with varying centre of mass position l_r, using an idealised driver model or a model incorporating sensory dynamics.

4.3.2 Vehicle optimisation performed in a driving simulator compared to a real car

Validation and optimisation of vehicle systems is increasingly being aided by test drivers in driving simulators. The driver model can be used to determine whether the optimal vehicle design determined in a simulator differs from the optimal design of a real vehicle. The optimisation procedure described in 4.3.1 is repeated with different scaling or filtering applied to the vehicle motion, and compared with the full motion results shown in Fig. 12. The motion conditions tested are full motion, no motion (to represent a fixed-base simulator), scaled motion (with $H_{ma}(s) = 0.2$ and $H_{m\omega}(s) = 0.2$) and filtered motion (with $H_{ma}(s) = 0.2H_{HP}(s)$ and $H_{m\omega}(s) = 0.2H_{HP}(s)$, where $H_{HP}(s)$ is a high-pass filter with a cutoff frequency of 5 rad/s [19]). In addition, simulations are carried out with filtered motion where the internal model motion filters are replaced with ESFs, as described in Section 4.2.3. The results using the idealised driver model do not depend on the motion scaling or filtering, therefore only the driver model with sensory dynamics is used.

The results of the simulations with different motion conditions are compared in Fig. 13. In general the differences between the motion conditions are very small, and far less significant than the effect of providing full state feedback seen in Fig. 12. The expected path-following error is slightly higher with no motion, indicating that results found in a fixed-base simulator may not be exactly the same as a real car. The driver's performance with scaled motion is exactly

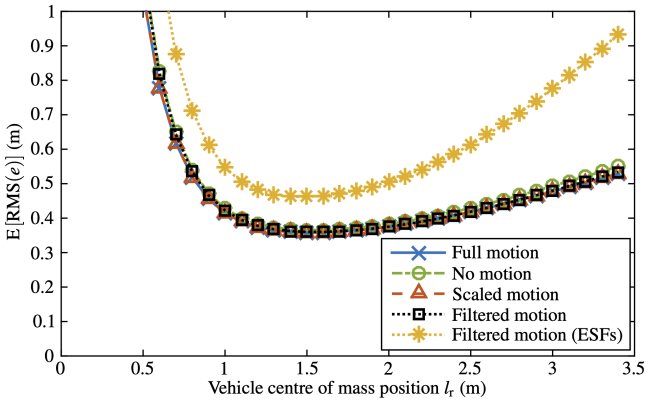

Fig. 13. Optimal centre of mass position with various motion conditions

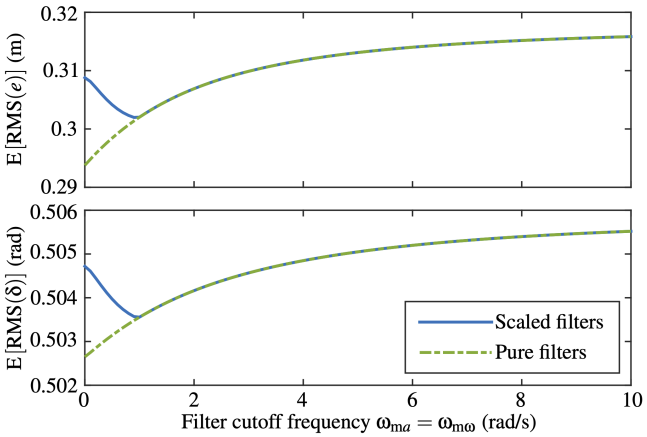

Fig. 14. Expected RMS path-following error e and steering angle δ, with sensory cancellation of responses to target-following control actions, for various cutoff frequencies

the same as with full motion as long as the motion is above threshold levels, as seen in Fig. 8. If the driver is able to develop an accurate internal model of the motion filters, the results for filtered motion lie between the full motion and no motion results. However, if the driver's internal model is inaccurate the results found in the simulator may be significantly different to the real car, as shown by the model with ESFs in Fig. 13. However, for the conditions tested the optimal value of l_r is similar for all cases. For a different scenario it is possible that an inaccurate internal model could have a greater effect on the optimal vehicle design.

5 Discussion

Predictions from the driver model in Section 4.2.2 indicate that scaling the physical motion in a simulator does not affect the driver's control performance, as long as the RMS signal amplitudes are above threshold levels. This implies that a driver in a simulator with scaled motion of sufficient amplitude should drive exactly as they would in a real vehicle. In reality, simulator motion is usually high-pass filtered, allowing the driver to feel more high-frequency motion while removing the low frequencies that quickly use up simulator travel. Figure 9 shows that the driver's performance can be improved by removing some of the lowest frequencies, however it also implies that scaling this filtered motion would have no effect on the driver. The reason for this is that the measurement noise amplitude increases in proportion to the overall signal RMS, resulting in a measurement with the same level of reliability independent of the scaling.

This signal-dependent noise characteristic was measured from experimental data in [12], and it is consistent with perception tests carried out in the literature [24–28]. However, these studies generally focussed on sinusoidal stimuli with a single frequency. Driving a real vehicle involves a large amount of low-frequency motion, due to the large steady-state accelerations involved in cornering, however this is superposed with higher-frequency motion caused by disturbances and the driver's steering responses. Since the driver model relates the noise amplitude to the RMS signal amplitude, the large steady-state components result in a large noise level, which causes the simulated driver to have difficulty perceiving small variations around the steady state. However in reality drivers are observed to be sensitive to these small high-frequency changes.

There are various possible reasons for this mismatch between the predictions of the model and what is observed in reality. Firstly, the model assumes that the measurement noise PSD is constant at all frequencies, however [11] shows that this results in an underestimation of low-frequency driver noise and an overestimation of high-frequency driver noise. Noise amplitudes are calculated based on the RMS value of the overall signal, however it may be more appropriate to relate the noise amplitude at each frequency to the corresponding signal amplitude at that frequency. Alternatively, the discrepancy could result from sensory adaptation effects. Humans have been found to adapt to low frequency motion under some conditions [29], and various studies have identified the effects of 'sensory cancellation', whereby humans are less sensitive to self-generated stimuli [30,31]. This could explain why large-amplitude signals from the target-following feedforward control, which are self-generated by the driver's control actions, do not disproportionately affect high-frequency disturbance perception.

A simple method for modelling these sensory cancellation effects is to ignore the target-following component in the calculation of the driver noise amplitudes. This method is used to run simulations similar to those presented in Section 4.2.2, accounting for sensory cancellation. The results are shown in Fig. 14, and they are closer to what would be expected than the previous results shown in Fig. 9. For pure motion filters (that is, high-pass filters without scaling) the best performance is now achieved with full motion (zero cutoff frequency), since the large amplitude low-frequency target-following motion is no longer present to dominate the RMS signal amplitude. The scaled filters perform worse at low cutoff frequencies due to the scaling of the perceived motion signals, bringing them below the threshold level. Similar results can be found by high-pass filtering the sensory signals before calculating the signal and noise amplitudes.

6 Conclusion and Further Work

A previously reported parametric driver steering model with sensory dynamics (visual and vestibular) has been used to give novel insight to the role of sensory dynamics in a target-path-following task in the presence of sensorimotor noise and random motion disturbances on the vehicle.

The visual system is found to be the dominant sensory system, with the influence of vestibular measurements increasing with the proportion of random disturbances on the vehicle. This result from the model explains the experimental finding in [15]. If the physical motion is scaled down (as might be experienced in a driving simulator) the weightings of the sensory measurements are not affected until the motion perception thresholds are reached.

State and tyre slip angle perception errors in a pure target-following task are around 10% in terms of RMS values, but increase significantly with the proportion of random disturbances on the vehicle. These findings from the model provide new insight to the role of sensory feedback and state estimation in driver perception

The model reveals that the driver's control bandwidth for target following is about 15 rad/s, depending on the steering cost weight in the controller. Vehicle motion disturbance rejection at mid-range frequencies is sacrificed to focus on low-frequency signals ($<$2rad/s) which affect the vehicle lateral displacement most significantly.

The driver's simulated control performance is unchanged with signal amplitude above perception threshold levels, although it is slightly affected by high-pass filtering of the physical motion such as might be experienced in a driving simulator. Large amplitude low-frequency or steady-state components of motion result in large noise level, which causes the simulated driver to have difficulty perceiving small variations around the steady state. However in reality drivers are observed to be sensitive to these small high-frequency changes.

Simulations were carried out with a simple internal model discrepancy, to represent a driver with incomplete understanding of the high-pass filtering of physical motion in a moving-base driving simulator. The driver model showed that path following performance is reduced in this case. These results from the model provide new insight to the finding in [12, 19] that drivers in a moving-base simulator may not always correctly account for high-pass filtered motion, and instead drive as though the motion were scaled.

The sensory driver model led to a significantly different optimum value of vehicle centre of mass position compared to that obtained using an idealised driver model. This result motivates the adoption of sensory driver models in a vehicle design setting; it was not clear from previously published work whether this would be the case. A similar optimisation task was performed using only the sensory driver model but comparing different motion conditions, as might be experienced in a driving simulator. It was found that the optimum centre of mass position did not depend significantly on the motion feedback condition, however this might not be the case for other design tasks.

Further work could be undertaken to improve the sensorimotor noise model, and to understand the nature of drivers' internal model errors. Although the driver model employed in this work has been extensively identified and validated against driving simulator experiments, some of the specific scenarios explored in this paper could be the basis of further experimental verification of the driver model.

Acknowledgements

This work was supported by the UK Engineering and Physical Sciences Research Council (EP/P505445/1, studentship for Nash). Supporting data are available at https://doi.org/10.17863/CAM.9741

References

[1] MacAdam, C. C., 2003. "Understanding and modeling the human driver". *Vehicle System Dynamics,* **40**(1-3), pp. 101–134.

[2] Plöchl, M., and Edelmann, J., 2007. "Driver models in automobile dynamics application". *Vehicle System Dynamics,* **45**(7-8), pp. 699–741.

[3] MacAdam, C. C., 1981. "Application of an optimal preview control for simulation of closed-loop automobile driving". *IEEE Transactions on Systems, Man, and Cybernetics,* **SMC-11**(6), pp. 393–399.

[4] Sharp, R. S., and Valtetsiotis, V., 2001. "Optimal preview car steering control". *Vehicle System Dynamics,* **35**(Suppl.1), pp. 101–117.

[5] Cole, D. J., Pick, A. J., and Odhams, A. M. C., 2006. "Predictive and linear quadratic methods for potential application to modelling driver steering control". *Vehicle System Dynamics,* **44**(3), pp. 259–284.

[6] Cole, D. J., 2017. "Occupant-vehicle dynamics and the role of the internal model". *Vehicle System Dynamics,* **56**(5), pp. 661–688.

[7] Keen, S. D., and Cole, D. J., 2011. "Application of time-variant predictive control to modelling driver steering skill". *Vehicle System Dynamics,* **49**(4), pp. 527–559.

[8] Tavernini, D., Velenis, E., Lot, R., and Massaro, M., 2014. "The optimality of the handbrake cornering technique". *ASME Journal of Dynamic Systems, Measurement, and Control,* **136**(041019), pp. 1–11.

[9] Nash, C. J., Cole, D. J., and Bigler, R. S., 2016. "A review of human sensory dynamics for application to models of driver steering and speed control". *Biological Cybernetics,* **110**(2-3), pp. 91–116.

[10] Nash, C. J., and Cole, D. J., 2017. "Modelling the influence of sensory dynamics on linear and nonlinear driver steering control". *Vehicle System Dynamics*.

[11] Nash, C. J., and Cole, D. J., 2020. "Identification and validation of a driver steering control model incorporating human sensory dynamics". *Vehicle System Dynamics,* **58**(4), pp. 495–517.

[12] Nash, C. J., and Cole, D. J., 2019. "Measurement and modelling of the effect of sensory conflicts on driver

steering control". *ASME J. Dyn. Sys., Meas., Control,* **141**(6), March, p. 11.

[13] Bruschetta, M., Cenedese, C., and Beghi, A., 2019. "A real-time, mpc-based motion cueing algorithm with look-ahead and driver characterization". *Transportation Research Part F,* **61**, pp. 38–52.

[14] Schwarzhuber, T., Graf, M., and Eichberger, A., 2021. "Investigations on model predictive control objectives for motion cueing algorithms in motorsport driving simulators". In IEEE Intelligent Vehicles Symposium (IV), Nagoya, Japan, July 11-17.

[15] Wolters, J. P. M. A., van der El, K., Damveld, H. J., Pool, D. M., van Paassen, M. M., and Mulder, M., 2018. "Effects of simulator motion on driver steering performance with various visual degradations". In IEEE International Conference on Systems, Man, and Cybernetics, Miyazaki, Japan, Oct 7-10.

[16] van der El, K., Pool, D. M., van Paassen, M. R. M., and Mulder, M., 2020. "A unifying theory of driver perception and steering control on straight and winding roads". *IEEE Transactions on Human-Machine Systems,* **50**(2).

[17] Markkula, G., Boer, E., Romano, R., and Merat, N., 2018. "Sustained sensorimotor control as intermittent decisions about prediction errors: computational framework and application to ground vehicle steering". *Biological Cybernetics,* **112**, pp. 181–207.

[18] Markkula, G., Romano, R., Waldram, R., Giles, O., Mole, C., and Wilkie, R., 2019. "Modelling visual-vestibular integration and behavioural adaptation in the driving simulator". *Transportation Research Part F,* **66**, pp. 310–323.

[19] Nash, C. J., and Cole, D. J., 2021. "Identification of a driver model incorporating sensory dynamics, with nonlinear vehicle dynamics and transient disturbances". *Vehicle System Dynamics,* **0**(0), pp. 1–20.

[20] Nash, C. J., 2018. "Measurement and modelling of human sensory feedback in car driving". Phd thesis, University of Cambridge.

[21] Nash, C., and Cole, D., 2020. "The role of human sensory dynamics in car driving". In Advances in Dynamics of Vehicles on Roads and Tracks, M. Klomp, F. Bruzelius, J. Nielsen, and A. Hillemyr, eds., Lecture Notes in Mechanical Engineering, IAVSD, Springer.

[22] Pick, A. J., and Cole, D. J., 2007. "Dynamic properties of a driver's arms holding a steering wheel". *Proceedings of the Institution of Mechanical Engineers, Part D: Journal of Automobile Engineering,* **221**(12), pp. 1475–1486.

[23] Pick, A. J., and Cole, D. J., 2008. "A mathematical model of driver steering control including neuromuscular dynamics". *Journal of Dynamic Systems, Measurement, and Control,* **130**(3), p. 031004.

[24] Weber, E., 1834. *Annotationes anatomicae et physiologicae*. CF Koehler.

[25] Authié, C. N., and Mestre, D. R., 2012. "Path curvature discrimination: Dependence on gaze direction and optical flow speed". *PLOS ONE,* **7**(2), p. e31479.

[26] Naseri, A. R., and Grant, P. R., 2012. "Human discrimination of translational accelerations.". *Experimental brain research,* **218**(3), pp. 455–464.

[27] Mallery, R. M., Olomu, O. U., Uchanski, R. M., Militchin, V. a., and Hullar, T. E., 2010. "Human discrimination of rotational velocities.". *Experimental brain research,* **204**(1), pp. 11–20.

[28] dos Santos Buinhas, L., Correia Grácio, B. J., Valente Pais, A. R., van Paassen, M., and Mulder, M., 2013. "Modeling coherence zones in flight simulation during yaw motion". In AIAA Modeling and Simulation Technologies Conference.

[29] Young, L. R., and Oman, C. M., 1969. "Model for vestibular adaptation to horizontal rotation.". *Aerospace medicine,* **40**(10), pp. 1076–1080.

[30] Lally, N., Frendo, B., and Diedrichsen, J., 2011. "Sensory cancellation of self-movement facilitates visual motion detection". *Journal of Vision,* **11**(14), pp. 5.1–9.

[31] Bays, P. M., Flanagan, J. R., and Wolpert, D. M., 2006. "Attenuation of self-generated tactile sensations is predictive, not postdictive". *PLOS Biology,* **4**(2), pp. 281–284.